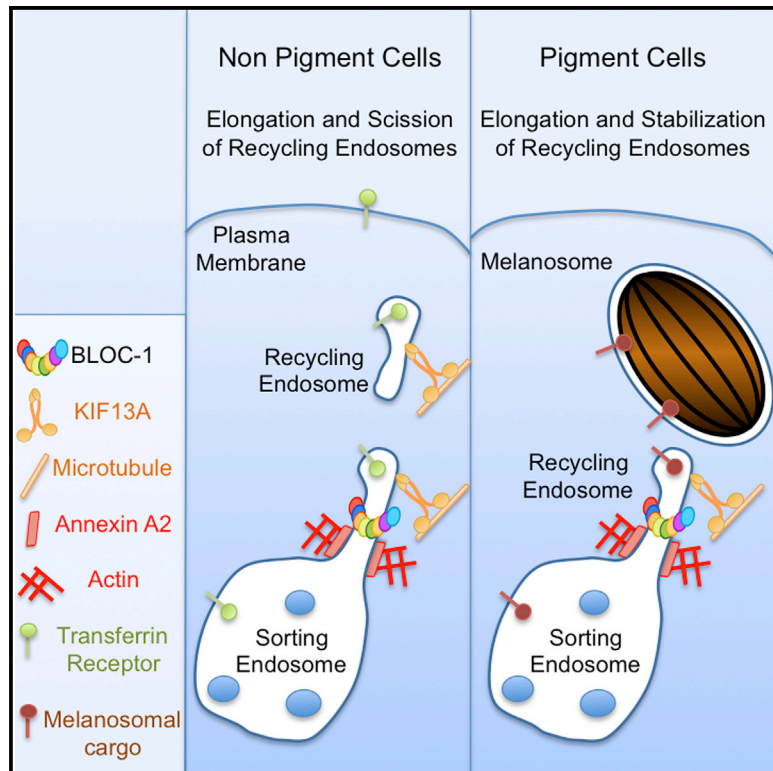# BLOC-1 Brings Together the Actin and Microtubule Cytoskeletons to Generate Recycling Endosomes

Graphical Abstract

Authors

Cédric Delevoye, Xavier Heiligenstein,
Léa Ripoll, ..., Victor Faundez,
Michael S. Marks, Graça Raposo

Correspondence

cedric.delevoye@curie.fr

In Brief

Delevoye et al. define the function of BLOC-1, mutated in neurological and pigmentary disorders. BLOC-1 forms recycling endosomes by orchestrating elongation and scission of tubules from sorting endosomes. By cooperating with microtubule (KIF13A) and actin (Annexin A2) components, BLOC-1 functions in cargo recycling and melanosome biogenesis.

Highlights

- BLOC-1 controls the formation of recycling endosomal tubules from sorting endosomes

- BLOC-1 cooperates with microtubule- and actin-associated machineries

- KIF13A and Annexin A2 are both required for the formation of recycling tubules

- Defects in recycling endosome biogenesis contribute to heritable disorders

CrossMark

CellPress

CellPress

BLOC-1 Brings Together the Actin and Microtubule Cytoskeletons to Generate Recycling Endosomes

Cédric Delevoye,[1,2,*] Xavier Heiligenstein,[1] Léa Ripoll,[1] Floriane Gilles-Marsens,[1] Megan K. Dennis,[3,4] Ricardo A. Linares,[3,4] Laura Derman,[1] Avanti Gokhale,[5] Etienne Morel,[6] Victor Faundez,[5] Michael S. Marks,[3,4] and Graça Raposo[1,2]

[1]Institut Curie, PSL Research University, CNRS, UMR144, Structure and Membrane Compartments, 75005 Paris, France
[2]Institut Curie, PSL Research University, CNRS, UMR144, Cell and Tissue Imaging Facility (PICT-IBiSA), 75005 Paris, France
[3]Department of Pathology and Laboratory Medicine, Children's Hospital of Philadelphia, Philadelphia, PA 19104, USA
[4]Department of Pathology and Laboratory Medicine and Department of Physiology, University of Pennsylvania, Philadelphia, PA 19104, USA
[5]Department of Cell Biology and the Center for Social Translational Neuroscience, Emory University, Atlanta, GA 30322, USA
[6]INSERM U1151-CNRS UMR 8253, Institut Necker Enfants-Malades (INEM) Université, Paris Descartes-Sorbonne Paris Cité Paris, 75993 Paris Cedex 14, France
*Correspondence: cedric.delevoye@curie.fr
http://dx.doi.org/10.1016/j.cub.2015.11.020

SUMMARY

Recycling endosomes consist of a tubular network that emerges from vacuolar sorting endosomes and diverts cargoes toward the cell surface, the Golgi, or lysosome-related organelles. How recycling tubules are formed remains unknown. We show that recycling endosome biogenesis requires the protein complex BLOC-1. Mutations in BLOC-1 subunits underlie an inherited disorder characterized by albinism, the Hermansky-Pudlak Syndrome, and are associated with schizophrenia risk. We show here that BLOC-1 coordinates the kinesin KIF13A-dependent pulling of endosomal tubules along microtubules to the Annexin A2/actin-dependent stabilization and detachment of recycling tubules. These components cooperate to extend, stabilize and form tubular endosomal carriers that function in cargo recycling and in the biogenesis of pigment granules in melanocytic cells. By shaping recycling endosomal tubules, our data reveal that dysfunction of the BLOC-1-KIF13A-Annexin A2 molecular network underlies the pathophysiology of neurological and pigmentary disorders.

INTRODUCTION

The early endosomal system comprises a membrane network from which biosynthetic and internalized components are sorted and trafficked among multiple target compartments in all eukaryotic cells. Proper sorting and trafficking within this network is necessary to maintain cellular homeostasis and to effect ubiquitous functions (e.g., cell polarity, migration, cytokinesis, and signaling) and cell type-specific functions (e.g., glucose metabolism, neurotransmitter storage, and pigmentation). Transmembrane cargoes within early endosomes are sorted from vacuolar sorting endosomes (SEs) or recycling endosomes (REs) [1]. REs comprise a network of interconnected and functionally distinct tubular subdomains that originate from SEs and transport their cargoes along microtubule tracks [2]. RE tubules ferry contents to the plasma membrane and the *trans*-Golgi network (TGN) in all cells or to lysosome-related organelles (LROs) in specialized cell types [3, 4].

The formation and stabilization of RE tubules from SE vacuoles requires the coordination of numerous effectors [5]. Membrane curvature at SE membranes is induced and/or stabilized by cytosolic coats and associated proteins [5]. Myosin motors on membrane-associated actin filaments then generate forces necessary to elongate the necks of nascent tubules. Actin nucleators, including the ARP2/3 complex regulated by endosome-associated WASH [6] and Spire1-Annexin A2 (AnxA2) complexes [7], generate branched actin filaments on endosomes. BAR-domain-containing scaffolds such as sorting nexins stabilize curvature on newly formed RE tubules [8], but tubule elongation is likely sustained by the microtubule-based motors, dynein and kinesins [9]. How the actin- and microtubule-associated machineries are coordinated in this process is not yet understood [5].

Specialized cell types like skin melanocytes provide a unique model for the biogenesis and function of the recycling endosomal system. Melanocytes modulate their endosomal pathway to generate melanosomes, LROs in which melanin pigments are synthesized and stored [10]. Defects in the trafficking of melanosomal cargoes (e.g., TYRP1) from endosomes to melanosomes during melanosome biogenesis underlie oculocutaneous albinism in the heritable disease Hermansky-Pudlak Syndrome (HPS) [11]. In particular, in HPS models (HPS7, HPS8, and HPS9) that lack BLOC-1 (biogenesis of lysosome-related organelle complex 1), TYRP1, and other melanosomal cargoes are trapped in enlarged SEs and fail to reach melanosome precursors [12–15], leading to impairment of pigmentation [11]. The precise role for BLOC-1 in cargo export from SEs is unknown. BLOC-1 localizes to endosomal tubules [16] and adopts a structure reminiscent of curved membrane-binding proteins [17], suggesting a potential role in stabilizing tubules.

The kinesin-3 motor, KIF13A, also facilitates the delivery of melanosomal cargoes by generating and transporting RE tubules that fuse ultimately with melanosomes [12]. Impaired KIF13A function phenocopies the hypopigmentation of BLOC-1-deficient melanocytes [12], suggesting that both may function in the same process. Moreover, genetic variations in KIF13A or BLOC-1 subunits appear to predispose to neurological disorders like schizophrenia [18–20].

Here, we show that BLOC-1 coordinates the action of microtubule- and actin-dependent machineries to elongate, stabilize, and ultimately release RE tubules. The molecular linkage between actin and microtubule cytoskeletons by BLOC-1 explains the molecular defect in HPS.

RESULTS

BLOC-1 Is Required for Recycling Endosome Tubule Biogenesis

The eight-subunit BLOC-1 is destabilized by loss of expression of the Pallidin, Muted, or Snapin subunits [21–23]. We investigated whether BLOC-1 supports RE tubule formation by quantifying KIF13A-positive (KIF13A$^+$) endosomal tubules in HeLa cells treated with a collection of siRNAs (small interfering RNAs) to these subunits (BLOC-1 siRNA), which effectively reduced expression of Pallidin, Muted, and the non-siRNA-targeted Dysbindin subunits relative to a control siRNA (Figure 1A). By live fluorescence imaging of HeLa cells treated with control siRNA, KIF13A-YFP (KIF13A) was detected in long RE tubules (arrows) that extended toward the cell periphery and were labeled by internalized transferrin-Alexafluor546 conjugates (TfA546; Figures 1B, S1A, and S1B; Movie S1; [24]). In contrast, BLOC-1-depleted cells accumulated KIF13A in enlarged, round, and mostly static TfA546$^+$ endocytic structures that were devoid of tubules (Figures 1B and S1C–S1F, arrowheads; Movie S2). Discrete KIF13A$^+$ and TfA546$^+$ structures emanated from these endosomes but did not elongate or detach over 1 min (Figures S1D and S1F; Movie S3). A small fraction of KIF13A$^+$ tubules (likely the least dynamic population) was stable to chemical fixation; by immunofluorescence microscopy (IFM), the percentage of cells that harbored at least one such KIF13A$^+$ tubule was ~40% reduced in BLOC-1-depleted cells relative to controls (Figure 1C). This likely underestimated the defect in these cells since most KIF13A$^+$ tubules—as described generally for early endosomal tubules [25]—are sensitive to aldehyde fixation [24]. Indeed, by live cell microscopy analysis (Figures 1D and 1E), the average number of dynamic KIF13A$^+$ tubules was dramatically decreased by BLOC-1 depletion. Moreover, the detected tubules were significantly shorter (Figure 1F), indicating a defect in RE tubule elongation. Whereas KIF13A segregated from SE in control cells and thus did not co-localize with SE-associated RAB5 (arrowheads), KIF13A co-distributed with RAB5$^+$ and Tf$^+$ SEs in BLOC-1-depleted cells (Figure 1G, arrows). This result supports our earlier data that RE tubules emerge from SE vacuolar domains in melanocytes [12, 26] and indicates that the primary source of KIF13A$^+$ RE membranes is RAB5$^+$ SEs. Moreover, as in siKIF13A-treated cells [24], Tf recycling was consistently reduced after 40 min of chase in BLOC-1-depleted cells relative to controls (Figure S1G). These observations suggest that BLOC-1 acts upstream of KIF13A during RE tubule biogenesis from SE in HeLa cells.

BLOC-1 Promotes Elongation of Nascent Recycling Endosomal Tubules

To better define the organelles from which RE tubules emanate and how they are controlled by BLOC-1, we analyzed cells by correlative light and electron microscopy (CLEM). KIF13A-YFP-expressing, BLOC-1-depleted HeLa cells that had internalized TfA546 were immobilized by high-pressure freezing (HPF) and processed for EM (electron microscopy) (Experimental Procedures and [27]). Consecutive sections of 250 and 70 nm in thickness were analyzed. The thick section was screened by FM (fluorescence microscopy) for cells harboring large TfA546$^+$ and KIF13A$^+$ structures (Figures 2A and S2A, arrows) that accumulate upon BLOC-1 depletion (Figure 1B). Identified structures were tracked on the thin section (Figures 2B and S2B, arrows) on which FM and EM images were acquired and overlaid (Figures 2C and S2C). KIF13A$^+$ and TfA546$^+$ structures had morphological features of SEs—vacuolar structures (~400 nm in diameter) containing none or few intraluminal vesicles (ILVs) (Figures 2D, 2E, and S2D). These SEs harbored multiple short budding profiles (Figures 2D, 2E, and S2D; Movie S4; arrowheads and schematized in Figure 2F), sometimes associated with tubular necks (Figures 2D and S2D, arrows) that were devoid of an apparent clathrin coat, reflecting local deformations of the SE membrane. By contrast (Figure 1B), KIF13A and internalized Tf co-distributed to the periphery of siCTRL (control siRNA)-treated cells by FM (Figures S2E–S2G, arrows); these areas corresponded by EM to regions enriched in tubules and vesicles (≤100 nm in diameter) characteristic of REs (Figure S2H, boxes 1–3, arrowheads; [2]). Importantly, very few budding profiles were observed on SEs in siCTRL cells (Figure S2H, boxes 2 and 4, arrows and Figure S2I, arrowheads) showing that they accumulated only upon BLOC-1 depletion (Figures 2 and S2).

We evaluated the number and shape of budded structures on endosomes in CTRL- and BLOC-1-depleted cells investigated by CLEM. BLOC-1 depletion increased 3-fold the number of round buds on endosomes (Figures 2E and 2G, arrowheads) but did not affect the number of elongated budded structures (Figure 2D, box 1, arrow and Figure 2G) or the shape of the round buds (Figures 2E and 2H, arrowheads). If BLOC-1 were to promote bud formation by bending the SE limiting membrane or to promote RE tubule detachment, BLOC-1 depletion would either reduce the number of round buds or increase elongated buds, respectively. By contrast, the accumulation of round buds (Figure 2) and loss of tubules (Figure 1) suggests that those buds can neither elongate nor detach from the SE-limiting membrane. We thus conclude that BLOC-1 promotes the extension and maturation of round buds into recycling tubular carriers and may contribute later to their stabilization. Such a role for BLOC-1 in stabilizing elongated buds would be consistent with its curvilinear structure [17] and its localization to endocytic tubules [16].

BLOC-1 Controls Endosomal Tubule Formation in Melanocytes

As BLOC-1 and KIF13A are required in melanocytes to deliver newly synthesized melanogenic cargoes from SEs to maturing melanosomes [13–16, 28], and BLOC-1-deficient [14] or KIF13A-depleted melanocytes [12] accumulate enlarged vacuolar endosomes in which these cargoes are retained, we tested whether BLOC-1 controls RE tubule generation in melanocytes.
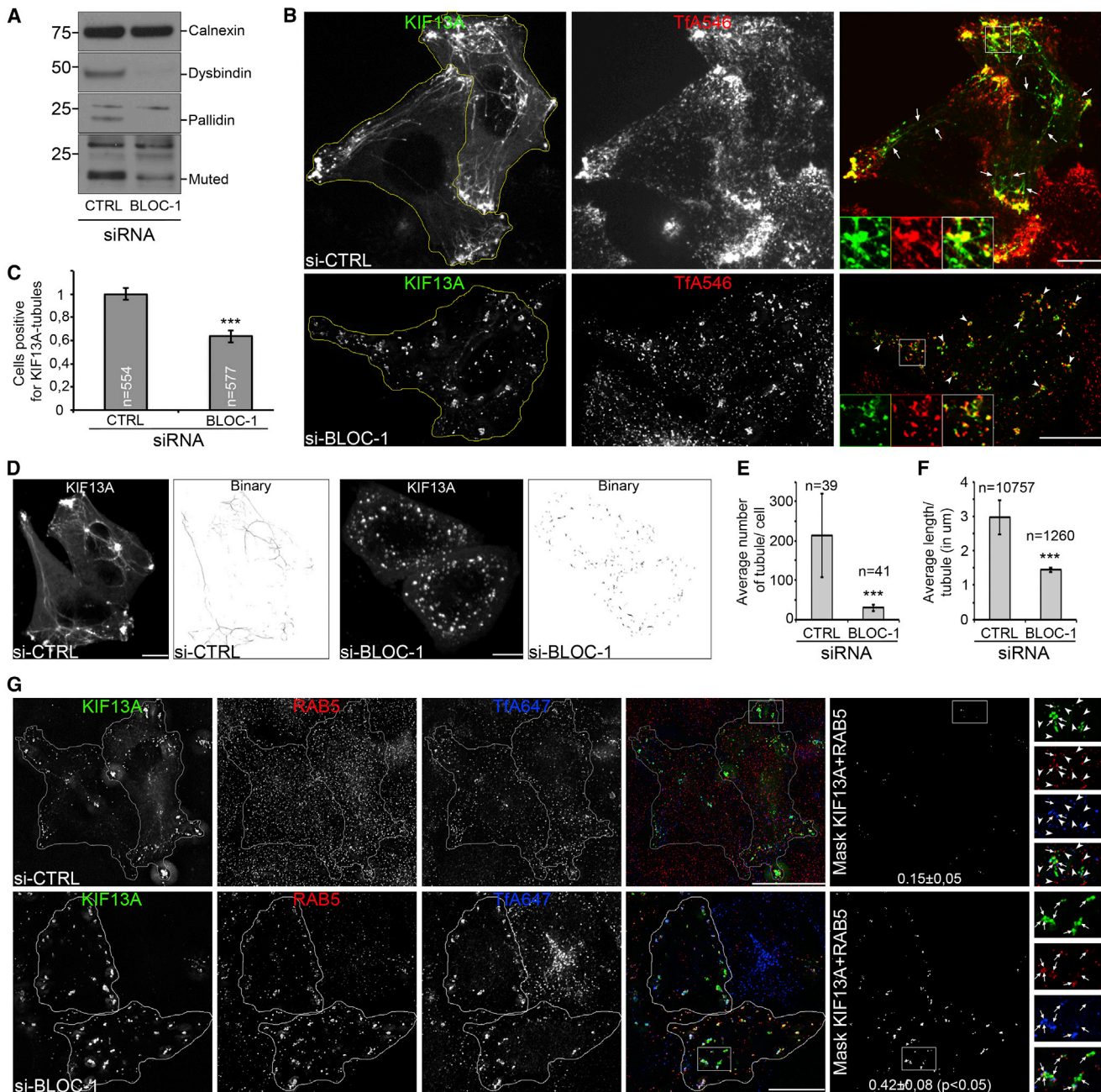
Figure 1. BLOC-1 Is Required to Generate Recycling Endosome Tubules

(A) Western blot (WB) of CTRL or BLOC-1 siRNA-treated HeLa cell lysates probed with antibodies to Dysbindin, Pallidin, Muted, or Calnexin.

(B) Live imaging frames of KIF13A-YFP-expressing siCTRL or siBLOC-1-treated cells that internalized TfA546. Arrows indicate KIF13A^{+} tubules in siCTRL cells; arrowheads indicate KIF13A in TfA546^{+} endosomes of siBLOC-1 cells (see Figure S1; Movies S1, S2, and S3).

(C) Quantification of the percentage of n siCTRL or siBLOC-1 cells generating at least one KIF13A^{+} tubule.

(D) Maximum projections of 3D stacks of live cell images of siCTRL or siBLOC-1-depleted cells and associated binary images after "skeletonize" processing.

(E) Quantification of the average number of tubules per n siCTRL or siBLOC-1 cells.

(F) Quantification of the average length (μm) per n tubules in siCTRL or siBLOC-1 cells.

(G) siCTRL or siBLOC-1 cells expressing KIF13A that internalized TfA647 were analyzed by IFM after labeling for RAB5. Co-localization masks and Pearson's coefficient are shown in the fifth column. Sixth column shows magnified boxed insets; arrows indicate co-distribution of KIF13A with RAB5 and Tf in siBLOC-1 cells; arrowheads indicate lack of overlap in siCTRL cells.

Data represent the average at least four independent experiments, normalized to control (C), and presented as mean ± SD (see Supplemental Information). ***$p < 0.001$. Molecular masses are in kD. Bars represent 10 μm.
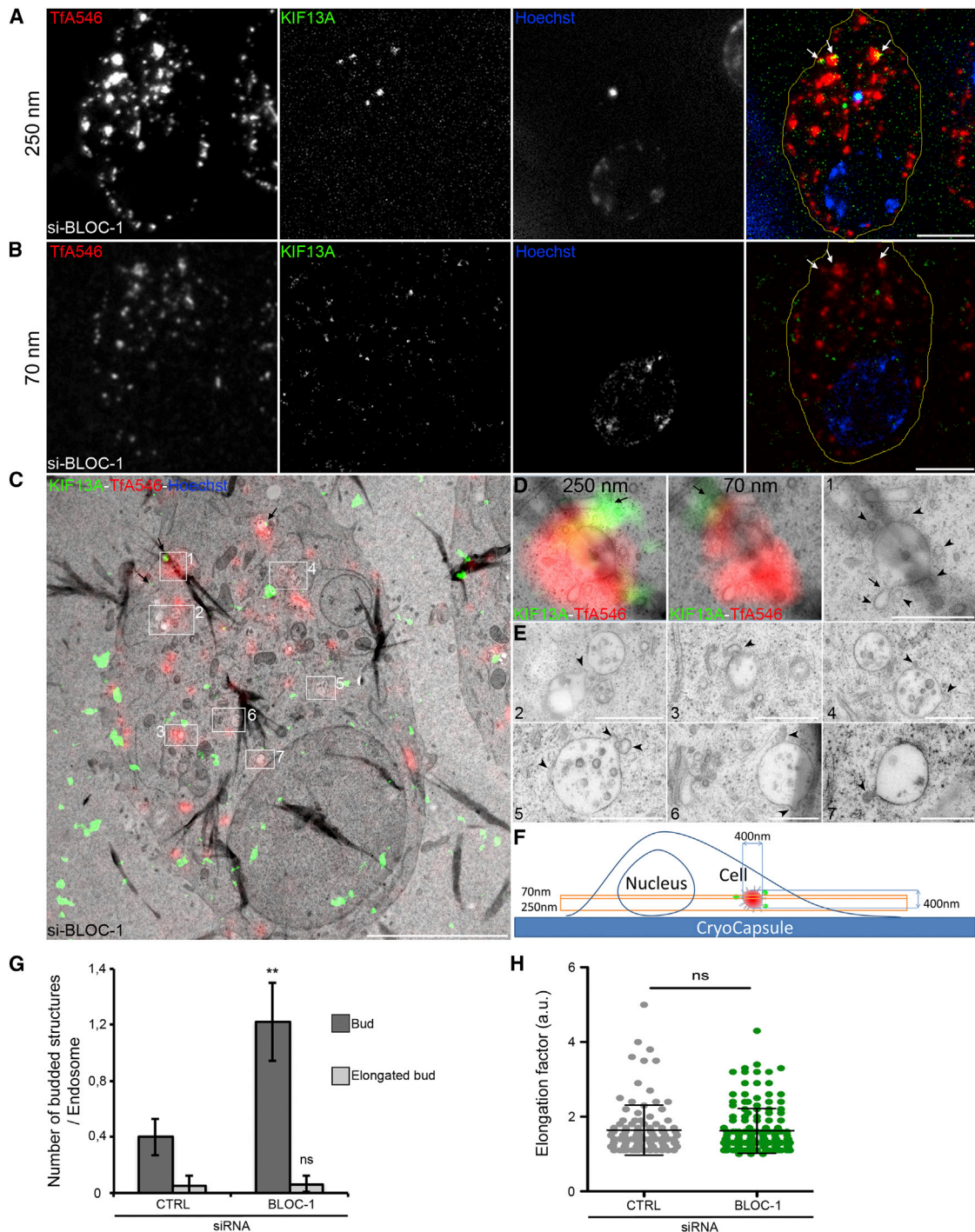
Figure 2. BLOC-1 Promotes Recycling Endosome Tubule Elongation

(A) High-pressure frozen siBLOC-1 HeLa cells analyzed by FM on the 250 nm thick section. Nucleus was stained with Hoechst (blue; bright dot, hole in the section). Arrows show large TfA546^{+} (red) and KIF13A^{+} (green) endosomes.

(B) Same endocytic structures (arrows) identified by FM on the consecutive thin section (70 nm). KIF13A (YFP) signal was barely detected and post-processed to increase signal-to-noise ratio.

(C) Overlay of the FM image (B) with the EM micrograph identifying the same endosomal structures (black arrows). White boxes show Tf[+] and KIF13A^{+} structures (box 1, panels in D) or Tf[+] endosomes (boxes 2–7, panels in E). Dark trails, folds in the section.

(D) Magnified insets of boxed area (1) merging the FM images acquired on 250 nm (left) or 70 nm (middle) sections. KIF13A localization was shifted along an endosomal tubule nearby SE (arrows). EM micrograph (right) shows buds or vesicles (arrowheads) associated to vacuolar SE containing ILVs. Arrow indicates cross-section of an elongated bud with a tubular neck emanating from SE.

(legend continued on next page)

REs labeled by transfected GFP-tagged syntaxin 13 (STX13) [29], as previously described [26], were detected by live cell imaging in BLOC-1-deficient (BLOC-1$^{-/-}$) melanocytes (melan-pa) derived from *pallid* mice or "rescued" melan-pa cells (BLOC-1^R) expressing the missing Pallidin subunit [14]. In BLOC-1^R melanocytes, STX13 labeled numerous cytoplasmic puncta and long tubules (Figures 3A and 3B, arrows). By contrast, STX13-labeled tubules were barely detected in BLOC-1$^{-/-}$ cells (Figure 3A, bottom panel, arrows), and those detected were significantly shorter than in BLOC-1^R cells (Figures 3A and 3B). Rather, BLOC-1$^{-/-}$ cells harbored enlarged and clustered STX13-labeled vacuoles (Figure 3A, arrowheads) similar to the SE vacuoles detected previously by EM [14]. These data indicate that BLOC-1 is required for the elongation of RE tubules out of SEs in different cell types.

BLOC-1 Cooperates with KIF13A in Melanosome Biogenesis

To test whether BLOC-1 and KIF13A cooperate within the same endosome-melanosome cargo transport pathways, we compared pigmentation and melanosome biogenesis in human MNT-1 melanocytic cells depleted of BLOC-1 or KIF13A alone or together. Cells treated with CTRL, BLOC-1, KIF13A, or BLOC-1 and KIF13A siRNAs resulted in specific depletion of KIF13A and/or BLOC-1 subunits (Figure 3C). By conventional EM, single depletion of either BLOC-1 or KIF13A caused a loss of mature pigmented stage III and IV melanosomes relative to controls (Figures S3A, S3B, and 3D, arrows) and a concomitant increase in immature and unpigmented stage I and II melanosomes (arrowheads), indicating a block in melanosome maturation as previously shown [12, 14]. Depletion of both BLOC-1 and KIF13A yielded an identical phenotype (Figure 3D) and a similar proportion of immature to mature melanosomes (Figure 3E). Accordingly, depletion of BLOC-1, KIF13A, or both decreased the intracellular melanin content by ~30% from control values (Figure 3F). The lack of a synergistic effect on either melanosome maturation or pigmentation suggests that BLOC-1 and KIF13A cooperate in the same cargo transport pathway.

We then tested whether BLOC-1 interacted physically with KIF13A. Whereas the endogenous BLOC-1 subunits Pallidin and Dysbindin were not enriched in anti-GFP immunoprecipitates (IPs) of HeLa cells expressing either GFP or YFP-KIF5B as controls, they were detected in IPs of cells expressing a GFP-tagged motor-deleted form of KIF13A (GFP-KIF13A-ST) (Figures 3G and S3C) that localizes to endosomes [24]. These data suggest that BLOC-1 and KIF13A associate within cells.

ARP2/3-Dependent Actin Polymerization Stabilizes Recycling Endosomal Tubules

Because actin polymerization can participate in the elongation, stabilization, and/ or fission of endosomal membranes [5], we investigated the role of actin dynamics in generating KIF13A-driven RE tubules. Brief incubation of KIF13A-expressing HeLa cells with the F-actin depolymerizing agent Latrunculin A (LatA) depleted actin fibers labeled by phalloidin-A546 (Figure 4A) and decreased by IFM the frequency of cells harboring at least one KIF13A RE tubule by ~25% relative to DMSO-treated cells (Figures 4A and 4B). LatA treatment showed a more dramatic reduction in dynamic tubule number and length (Figures 4C–4E), comparable to BLOC-1 depletion (Figures 1E and 1F), when analyzed by live cell imaging. In LatA-treated cells, KIF13A associated with enlarged (Figure 4A, arrows) and largely immobile (Movie S5) Tf$^+$ structures resembling those in BLOC-1-depleted cells (Figures 1B and S1C–S1F). Addition of LatA 5 min before video microscopy analysis revealed rapid retraction and collapse of KIF13A-containing tubules (Movie S5), showing that actin dynamics are required for optimal microtubule-dependent elongation of RE tubules [24].

To define the machinery that promotes actin polymerization during RE tubule formation, HeLa cells were analyzed after treatment with inhibitors of the ARP2/3 complex (CK-666) or formin family proteins (SMIFH2). Relative to vehicle (DMSO), CK-666, but not SMIFH2, reduced the frequency of cells with at least one KIF13A-RE tubule by ~25% by IFM (Figures 4B and 4F)—as much as LatA treatment—and dramatically decreased the number and length of dynamic KIF13A$^+$ tubules by live cell imaging (Figures 4C–4E). As with LatA, CK-666-treated cells harbored enlarged KIF13A$^+$ structures despite no general effect on actin fibers (Figure 4F, top panels, arrows). In contrast, SMIFH2-treated cells still generated KIF13A-labeled tubules (Figure 4F, bottom panels, arrows) that were transported toward the cell periphery (arrowheads) like in control cells (Figures 4A and 4C, top panels). Peripheral KIF13A-containing puncta that were observed in control cells by IFM and live imaging (Figures 4A and 4C, arrowheads and [24]) were abolished by combined treatment with nocodazole and LatA or CK-666, then restored upon washout of all drugs, but not upon washout of the actin drugs alone (Figure 4G). This shows that ARP2/3-dependent actin polymerization alone, in the absence of microtubules, is not sufficient to elongate RE tubules. Our data together show that ARP2/3-dependent but formin-independent actin polymerization is required for the stabilization of KIF13A-RE tubules.

ARP2/3-dependent actin polymerization requires activation. The WASH complex activates ARP2/3 on endosomes [6] following its recruitment by retromer [30], but our data do not support a role for WASH in KIF13A-dependent RE tubule formation. First, whereas KIF13A co-distributed by IFM with AP-1 [12] or internalized Tf [24] (arrows), it did not co-localize significantly with WASH or the VPS35 subunit of retromer (arrowheads) (Figure S4A). Second, siRNA depletion of WASH or the retromer subunit VPS35 in KIF13A-expressing cells did not affect the generation of KIF13A-RE tubules (Figures S4B–S4D, arrows). Third, WASH depletion in melanocytic cells did not impair pigmentation like KIF13A or BLOC-1 depletion (Figure S4E; compare to Figure 3F), indicating that WASH is not required for melanosome maturation. Thus, RE tubule stabilization and/or fission requires

(E) Magnified insets of boxed areas (2–7). Heavily (2–3) or faintly (4–7) TfA546$^+$ endosomes corresponded to SEs harboring budded profiles (arrowheads).
(F) Diagram of a cell grown on CryoCapsule and of the thin and thick sections related to the size of fluorescent endosomes. Several budding profiles observed on thin section suggest that endosomal surface is covered by membrane deformations (see Movie S4).
(G) Quantification of the number of bud and elongated bud structures on endosomes by CLEM.
(H) Elongation factor of buds in siCTRL and siBLOC-1 cells.
Data represent mean ± SD; ns, non-significant; **p < 0.01. Scale bars represent 5 μm (FM); 5 μm (EM, C); 500 nm (EM, D–E).
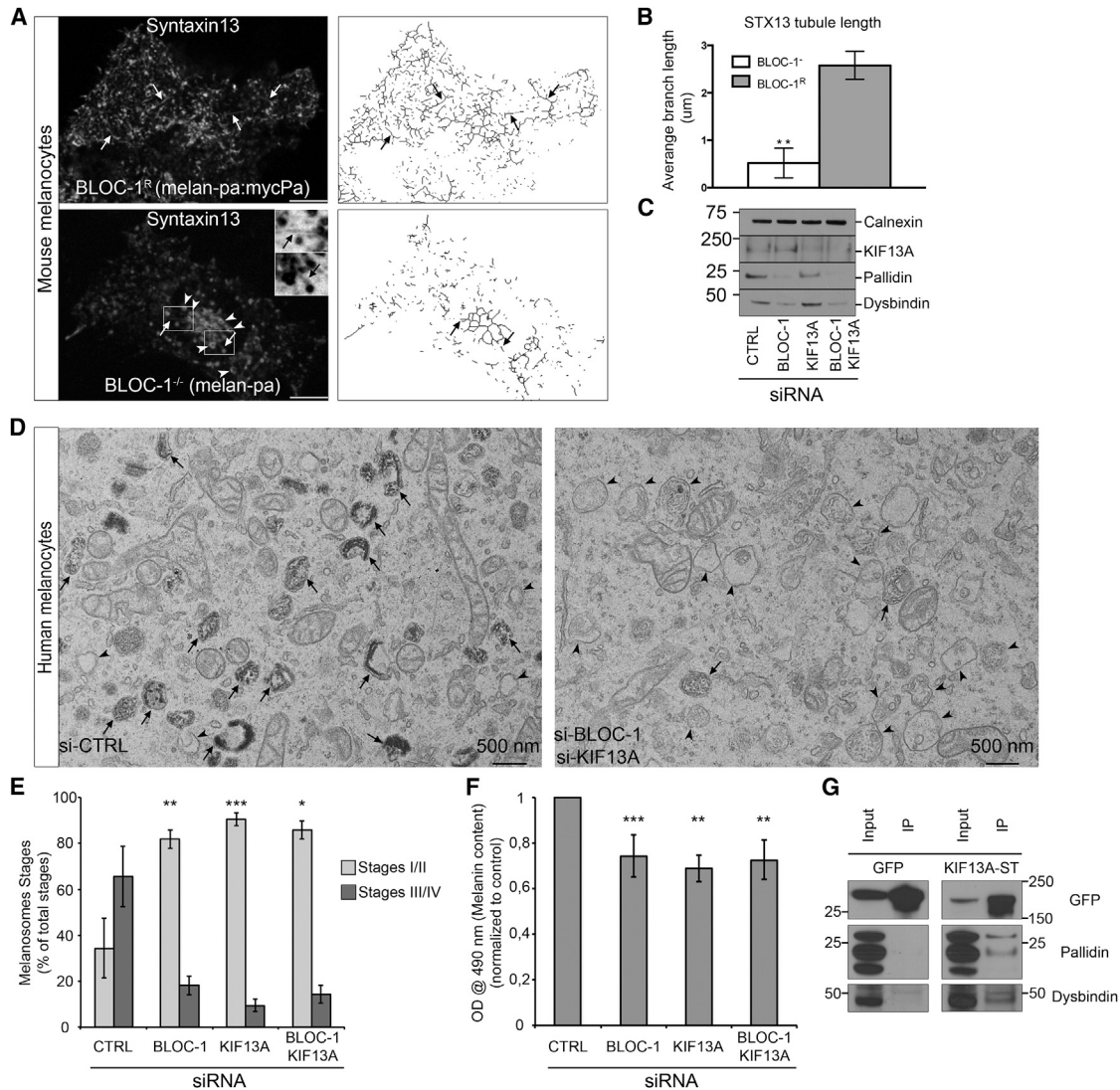
Figure 3. BLOC-1 and KIF13A Cooperate for Melanosomes Biogenesis

(A) Live cell spinning disk confocal microscopy analysis of immortalized BLOC-1-deficient (BLOC-1$^{-/-}$; melan-pa1; bottom) or "rescued" (BLOC-1^R; melan-pa1:mycPa; top) mouse melanocytes expressing GFP-Syntaxin13 (STX13). Shown are individual frames before (left) or after (right) "skeletonize" processing. Arrows indicate STX13$^+$ tubules; arrowheads indicate enlarged vacuolar endosomes in BLOC-1$^{-/-}$ cells.

(B) STX13 tubule length was measured (mean ± SD) as the branch length in skeletonized frames.

(C) WB of human MNT-1 melanocyte lysates depleted for BLOC-1, KIF13A, or both together.

(D) Conventional EM analysis of siCTRL or siBLOC-1 and siKIF13A MNT-1 cells. Arrowheads indicate immature melanosomes; arrows indicate mature pigmented melanosomes.

(E) Quantification of immature melanosomes (stages I/II) and mature melanosomes (stages III/IV) per condition.

(F) Melanin content estimation of cells treated with CTRL, BLOC-1, KIF13A, or both siRNAs.

(G) WB of GFP immunoprecipitations (IPs) of GFP- or GFP-KIF13A-ST-expressing HeLa cell lysates analyzed using GFP (top), Pallidin (middle), or Dysbindin (bottom) antibodies.

Data represent the average of at least three independent experiments, normalized to control (F), and presented as mean ± SD (see Supplemental Information). ***p < 0.001; **p < 0.01; *p < 0.05. Scale bars represent 10 μm (IFM) and 500 nm (EM). Molecular masses are in kD.

the ARP2/3-dependent but WASH-independent local polymerization of branched actin filaments, likely on SE membranes.

AnxA2 Is Required to Generate Recycling Endosomal Tubules

We next tested whether AnxA2 serves as an alternative to WASH in ARP2/3 activation during RE tubule formation. AnxA2 is a phospholipid binding protein [31] that initiates ARP2/3-dependent actin polymerization on early endosomal membranes [7]. Consistent with the detection of AnxA2 on endosomal tubules [32, 33], endogenous AnxA2 decorated KIF13A$^+$ tubules in HeLa cells (Figures 5A and 5B, arrows). Endogenous AnxA2 was co-immunoprecipitated with GFP-KIF13A-ST or GFP-KIF13A-T (containing only the KIF13A tail domain; [12]), but not
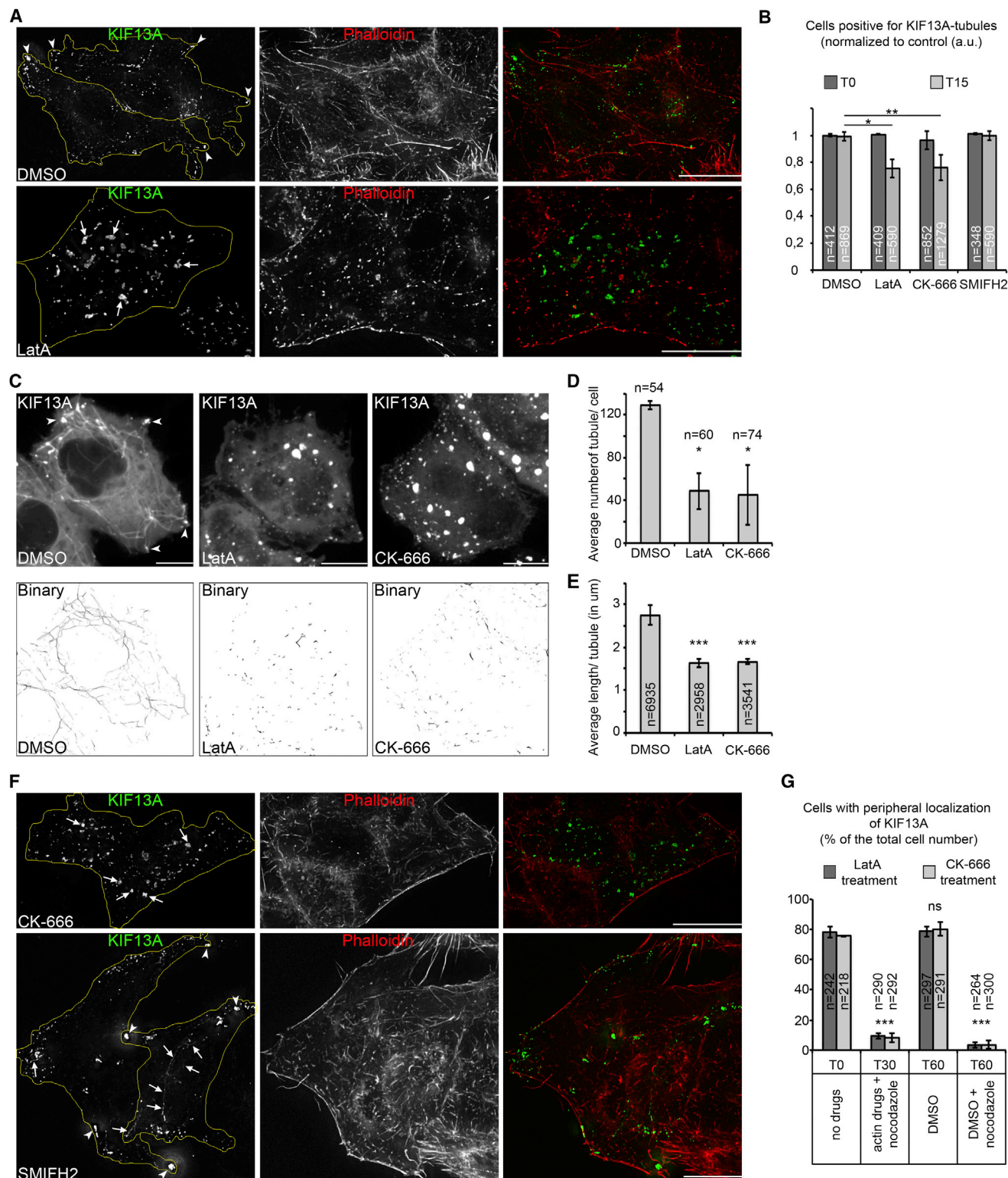
A

B

Cells positive for KIF13A-tubules
(normalized to control (a.u.))

C

D

E

F

G

Cells with peripheral localization
of KIF13A
(% of the total cell number)

Figure 4. Actin Dynamic and ARP2/3 Stabilize Recycling Tubules

(A) IFM on DMSO- or LatA-treated, KIF13A-expressing HeLa cells stained for F-actin (Phalloidin-A546). Arrows indicate KIF13A^{+} vesicular structures; arrowheads indicate KIF13A at cell periphery.

(B) Quantification of the percentage of DMSO-, LatA-, CK-666-, or SMIFH2-treated cells generating at least one KIF13A^{+} tubule.

with GFP alone, the melanosome-associated myosin VI motor [34], or the kinesin-1 KIF5B (Figures 5C, S5A, and S5B), indicating that AnxA2 associated physically with the KIF13A tail.

We then tested whether AnxA2 modulates RE function. In agreement with previous reports [35, 36], AnxA2 depletion by siRNA (Figure 5D) impaired Tf recycling as shown by higher intracellular Tf intensity after 40 min of chase relative to controls (Figure S5C). Moreover, as for BLOC-1 depletion or Arp2/3 inhibition, ∼20% fewer AnxA2-depleted cells harbored at least one KIF13A-RE tubule relative to controls (Figure 5E), the number and length of dynamic tubules by live cell imaging were dramatically reduced (Figures 5F and 5G), and KIF13A accumulated on enlarged Tf$^+$ and Rab5$^+$ SEs (Figures 5H and S5D, arrowheads). Thus, AnxA2 activity facilitates the generation of KIF13A-dependent RE tubules from SEs.

To characterize the effects of AnxA2 depletion on endosome morphology, AnxA2-depleted cells expressing KIF13A-YFP were analyzed by HPF-CLEM following TfA546 internalization. Cells harboring large KIF13A$^+$ (green) and Tf$^+$ (red) structures were identified by FM on 250 nm thick sections (Figure S5E, arrows), and the corresponding 70 nm thin sections were used for correlative image registration (Figures S5F and 5I, arrows). Like in BLOC-1-depleted cells, but not control cells (Figures 2 and S2), fluorescent structures in AnxA2-depleted cells corresponded to SEs containing ILVs from which several buds emanated (Figures 5J and S5G; Movie S6; arrowheads). Endosomes harbored slightly more rounded buds than controls, but most buds were elongated compared to those in CTRL- or BLOC-1-depleted cells (Figures 5J–5L and S5G; Movie S6; arrows). These tubular structures—defined as elongated buds—remained attached to the SE-limiting membrane and increased 8-fold relative to either CTRL- (Figures 5J and 5L, arrows) or BLOC-1-depleted cells (Figure 2G). These data suggest that AnxA2 functions downstream of BLOC-1 in the stabilization and/or scission of KIF13A-dependent RE tubules from the limiting membrane of SEs.

AnxA2 Cooperates with BLOC-1 on Endosomes

Although they cooperate functionally with KIF13A activity at the SE, attempts to demonstrate a physical association between AnxA2 and BLOC-1 were unsuccessful (data not shown). However, by IFM on siBLOC-1-treated HeLa cells, a cohort of AnxA2 co-distributed with KIF13A in Tf-containing endosomes (Figure 6A, arrows) rather than on RE tubules as in controls (Figure 5A, arrows). These endosomes likely corresponded to the SEs identified by CLEM in BLOC-1-depleted cells (Figures 2D, 2E, and S2D), indicating that BLOC-1 is not required to recruit AnxA2 to SEs. IFM and IEM (immuno-electron microscopy) ana-

lyses showed that endosomes in BLOC-1-inactivated cells were depleted of actin fibers (Figures S6A–S6C, arrows), indicating that the AnxA2 accumulated on these endosomes do not hyper-stimulate actin polymerization. Interestingly, the fraction of AnxA2 co-immunoprecipitated by KIF13A decreased in siBLOC-1-treated cells relative to controls (Figure 6B), suggesting that BLOC-1 stabilizes the interaction between KIF13A and AnxA2 and might promote the local association of AnxA2 with emanating REs. Additionally and like other BLOC-1-interacting proteins [37], long-term Pallidin shRNA (short hairpin RNA) treatment (Figures S6D and S6E, 7 days), but not short-term siBLOC-1 depletion (Figure 6C, lane 2; ∼3 days), reduced AnxA2 expression relative to controls, suggesting that BLOC-1 might also stabilize AnxA2. Thus, BLOC-1 functions upstream of AnxA2 with which it cooperates to control the elongation and/or scission of KIF13A$^+$ RE tubules from SEs.

Annexin A2 Cooperates with BLOC-1 and KIF13A in Melanosome Biogenesis

Since AnxA2 promotes BLOC-1- and KIF13A-dependent RE tubule formation in HeLa cells and similar RE tubules function in melanosome biogenesis in melanocytes, we addressed whether AnxA2 controls melanosome maturation. Relative to that of controls, the melanin content of AnxA2-depleted melanocytes was reduced by ∼20% (Figures 6C and 6D, lane 4), as observed in BLOC-1- or KIF13A-inactivated cells (Figures 6C and 6D). Concomitant depletion of AnxA2 and BLOC-1, KIF13A, or both did not further reduce pigmentation relative to cells depleted singly of BLOC-1 or KIF13A (Figures 6C and 6D), suggesting that AnxA2, BLOC-1, and KIF13A function within the same endosome-to-melanosome pathway. AnxA2-depleted melanocytes, like those depleted of BLOC-1 or KIF13A (Figures 3D, 3E, S3A, and S3B), had drastically fewer pigmented melanosomes than controls (arrows) and accumulated immature non-pigmented melanosomes (arrowheads) (Figures 6E and 6F). Thus, AnxA2 promotes melanosome maturation and pigmentation. The lack of additive effects with KIF13A and/or BLOC-1 depletion and the similarity of the phenotypes lead us to propose that AnxA2 cooperates with BLOC-1 and KIF13A to regulate the formation of tubular RE transport intermediates that function in melanosome biogenesis.

DISCUSSION

Recycling endosomes were identified three decades ago [2], but the molecular mechanisms underlying their formation remain poorly understood, likely owing to the functional redundancy of endosomal domains that can support the recycling of most studied cargoes [38]. Here, we detail key players in RE

(C) Maximum projections of 3D stacks of live cell images of DMSO-, LatA-, or CK-666-treated KIF13A-expressing cells and associated binary images (skeletonize). Arrowheads indicate KIF13A$^+$ structures at cell periphery.

(D) Quantification of the average number of tubules per n cells treated in (C).

(E) Quantification of the average length (in μm) per n tubules in cells treated in (C).

(F) IFM on CK666- or SMIFH2-treated, KIF13A-expressing HeLa cells stained for F-actin (Phalloidin-A546). Arrows indicate KIF13A$^+$ vesicular structures; arrowheads indicate KIF13A at cell periphery.

(G) Percentage of n cells with peripheral KIF13A$^+$ structures fixed before (T0), after (T30, actin drugs + nocodazole) 30 min incubation with LatA (dark gray bars) or CK-666 (light gray bars) with nocodazole, then after DMSO (30 min, T60 DMSO) or DMSO + nocodazole (30 min, T60 DMSO + nocodazole).

Data are presented as the average of two to four independent experiments, normalized to control (B), and presented as mean ± SD. *p < 0.05; **p < 0.01; ***p < 0.001. Scale bars represent 10 μm (IFM).
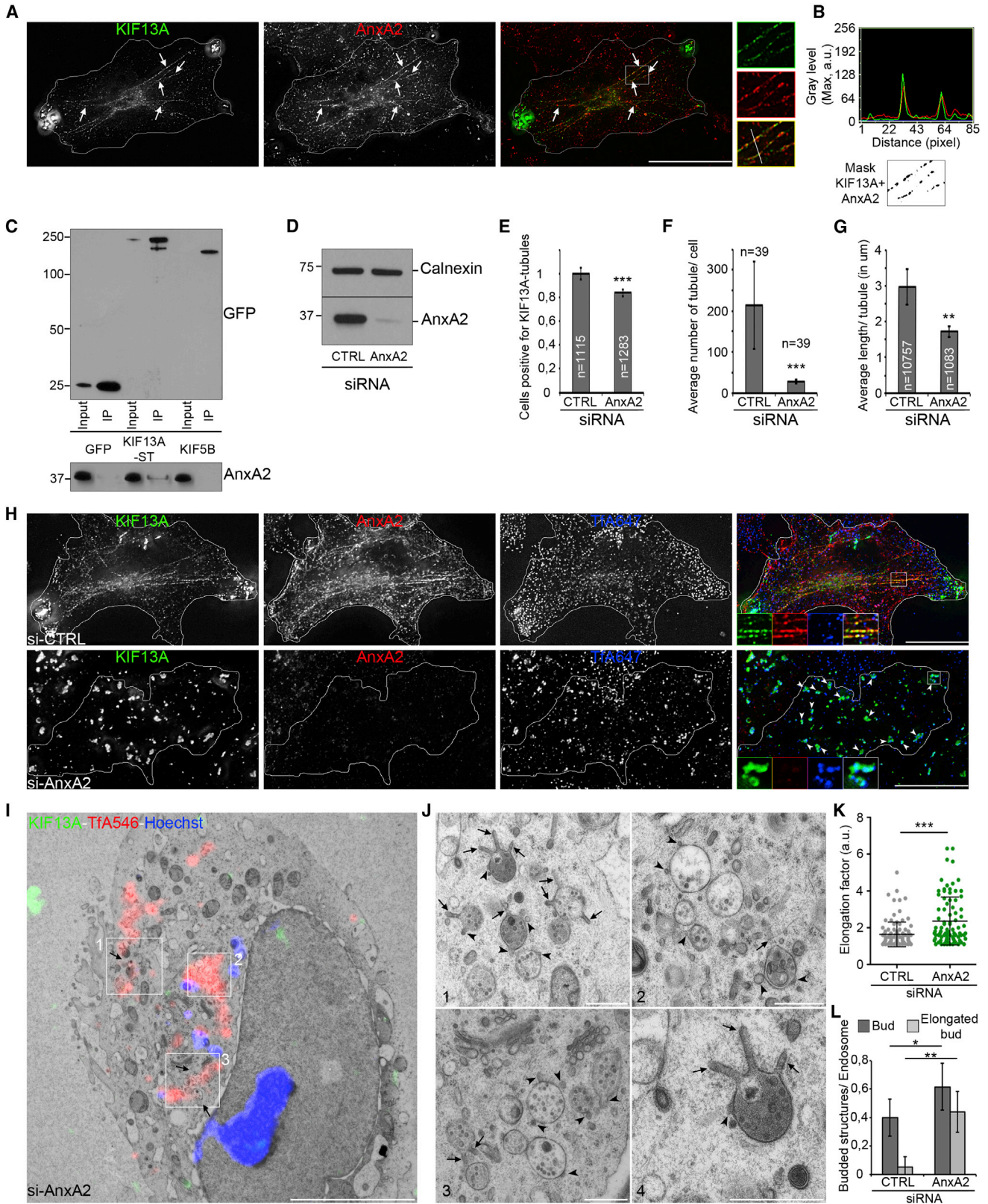
(legend on next page)

biogenesis by exploiting two functional readouts: the tubular morphology of REs in HeLa cells and RE-dependent melanosome maturation in melanocytic cells. Our results identify BLOC-1, a schizophrenia susceptibility factor and the target of mutation in HPS subtypes, as an endocytic module linking microtubule (KIF13A) and actin (AnxA2) cytoskeleton-related machineries to couple the remodeling of SE membranes to the generation, elongation, and scission of RE tubules.

RE tubule biogenesis starts with the generation of membrane curvature on SE membranes. Local membrane deformation can recruit membrane sensors, like BAR domain-containing proteins, that might stabilize and/or elongate nascent tubules. BLOC-1 might function as such a sensor for nascent RE tubules since recombinant BLOC-1 forms a curvilinear chain with a substantial bend by negative stain electron microscopy [17] and localizes to tubular endosomes by whole-mount EM [16]. Accordingly, the increased number of buds associated to endosomes in BLOC-1-depleted cells indicates that BLOC-1 functions downstream of the first remodeling event. We therefore propose that BLOC-1 is preferentially recruited to nascent RE buds where it functions as a molecular scaffold for further elongation of the RE tubule. The interaction of BLOC-1 with KIF13A—the first microtubule-associated motor identified to interact functionally and physically with BLOC-1—might then permit KIF13A to engage microtubules to initiate tubule elongation. The interaction of BLOC-1 with KIF13A mirrors the indirect association of the related BORC with Kinesin-1 to regulate motility of lysosomes [39] and might reflect an evolutionarily conserved function of the common BLOC-1 and BORC subunits. Interestingly, we also observed interactions of KIF17 with BLOC-1 and AnxA2 (unpublished data). KIF17 promotes cargo trafficking [40] to actin-rich synaptic regions in post-synaptic neurons [41]. One may speculate that the BLOC-1/AnxA2 module may engage other kinesins for additional broader functions.

The bending and elongation of the SE membrane must be supported and sustained by actin-driven mechanical forces, as proposed during endocytosis [42, 43]. We demonstrate that BLOC-1 cooperates with AnxA2 and Arp2/3 to stabilize RE tubules in HeLa cells and melanocytes. By favoring the interaction of AnxA2 with KIF13A, BLOC-1 functions upstream of both the microtubule- and actin-dependent machineries in the elongation

and stabilization of nascent RE tubules. Whereas BLOC-1 engages actin regulators such as WASH [21, 37, 44] in some cell types and WASH controls the trafficking of some BLOC-1-dependent cargoes [37], we show that BLOC-1 and WASH play distinct roles in RE tubule generation and melanosome biogenesis. The cooperation between BLOC-1 and WASH is likely dependent on cell type, endosomal subpopulation, and/or cargo.

BLOC-1 functions in RE biogenesis through AnxA2 to activate Arp2/3 to initiate branched actin filaments [7]. AnxA2 associates to early endosomes [32] and modulates endosomal dynamics and function along recycling [35, 36] and degradative pathways [45, 46]. AnxA2 depletion has also been shown to block early to late endosome maturation without affecting ILV formation [45]. Similar defects were observed upon KIF13A or BLOC-1 depletion [24, 47], whereas selected cargo sorting of PMEL (pigment cell-specific melanocyte protein) to ILVs was unaffected [12, 14]. These data suggest that AnxA2, BLOC-1, and KIF13A cooperate to regulate early to late endosome maturation. This is likely a consequence of their effects on RE tubule formation, as vacuolar SE and tubular RE are interconnected subdomains; therefore, impairing the formation of RE tubules would prevent SE-limiting membrane remodeling required for proper cargo sorting and endosome maturation [12, 24].

By linking actin and microtubule machineries, BLOC-1 is well suited to orchestrate the elongation and detachment of RE tubules from SE and thus to effect the sorting of cargoes destined for LROs in cells like melanocytes or for the plasma membrane or Golgi in other cell types. We propose a model of RE tubule biogenesis (Figure 6G) that incorporates our findings. First, membrane deformation of the flat SE membrane (1) generates a curved bud to which BLOC-1 associates (2). This facilitates KIF13A recruitment to SE subdomains (3), which promotes bud elongation along microtubules (4). Then, AnxA2 activates ARP2/3-dependent local polymerization of branched actin filaments (5) [7], stabilizing and allowing for the potential scission of the newly formed RE tubule. The tubule is then transported along the microtubule network toward its destination—the plasma membrane [24] or maturing melanosomes [12]—via KIF13A. In this model, KIF13A motor activity along microtubules generates the pulling force required to sustain tubule elongation

---

Figure 5. Annexin A2 and KIF13A Cooperate for Recycling Tubules Formation

(A) IFM of KIF13A-expressing (green) HeLa cells labeled with AnxA2 (red) antibody. Arrows indicate KIF13A^{+} and AnxA2^{+} RE tubules.

(B) Intensity profile of KIF13A (green) and AnxA2 (red) fluorescence along tubules (white line in A, merged panel box). Co-localization mask (bottom) of KIF13A^{+} and AnxA2^{+} pixels from the merged panel inset.

(C) WB of IP of GFP, GFP-KIF13A-ST, or YFP-KIF5B-expressing HeLa cells lysates analyzed using GFP (top) or AnxA2 (bottom) antibodies.

(D) WB of si-CTRL or si-AnxA2 HeLa cells lysates using AnxA2 or calnexin antibodies.

(E) Quantification of n siCTRL or siAnxA2 cells generating at least one KIF13A^{+} tubule.

(F) Quantification of the average number of tubules per n siCTRL or siAnxA2 cells.

(G) Quantification of the average length (in μm) per n tubules of siCTRL or siAnxA2 cells.

(H) IFM of siCTRL or siAnxA2, KIF13A (green) expressing HeLa cells labeled for AnxA2 (red) antibody that internalized TfA647 (blue). Arrowheads indicate KIF13A in Tf[+] vesicular endosomal structures. Magnified insets (boxed areas) of singles and merged panels are shown.

(I) CLEM on AnxA2-depleted HeLa cells expressing KIF13A that internalized TfA546. FM image on 70 nm section (see Figure S5F) overlaid to the EM micrograph. Arrows indicate correlated Tf[+] and KIF13A^{+} structures (see Figures S5E and S5F); white boxes indicate Tf[+] and KIF13A^{+} structures.

(J) Magnified insets (boxed areas) of SEs containing ILVs harboring buds (arrowheads) or elongated budding structures (arrows) in continuity with vacuolar domains (see Movie S6).

(K) Elongation factor of buds in siCTRL and siAnxa2 cells.

(L) Quantification of the number of bud and elongated bud structures on endosomes in siCTRL and siAnxa2 cells.

Data are presented as mean ± SD. Others represent the average of three independent experiments, normalized (E) to control, and presented as mean ± SD. *p < 0.05; **p < 0.01; ***p < 0.001. Molecular masses are in kD. Scale bars represent 10 μm (IFM), 5 μm (EM, G), and 500 nm (EM, H).
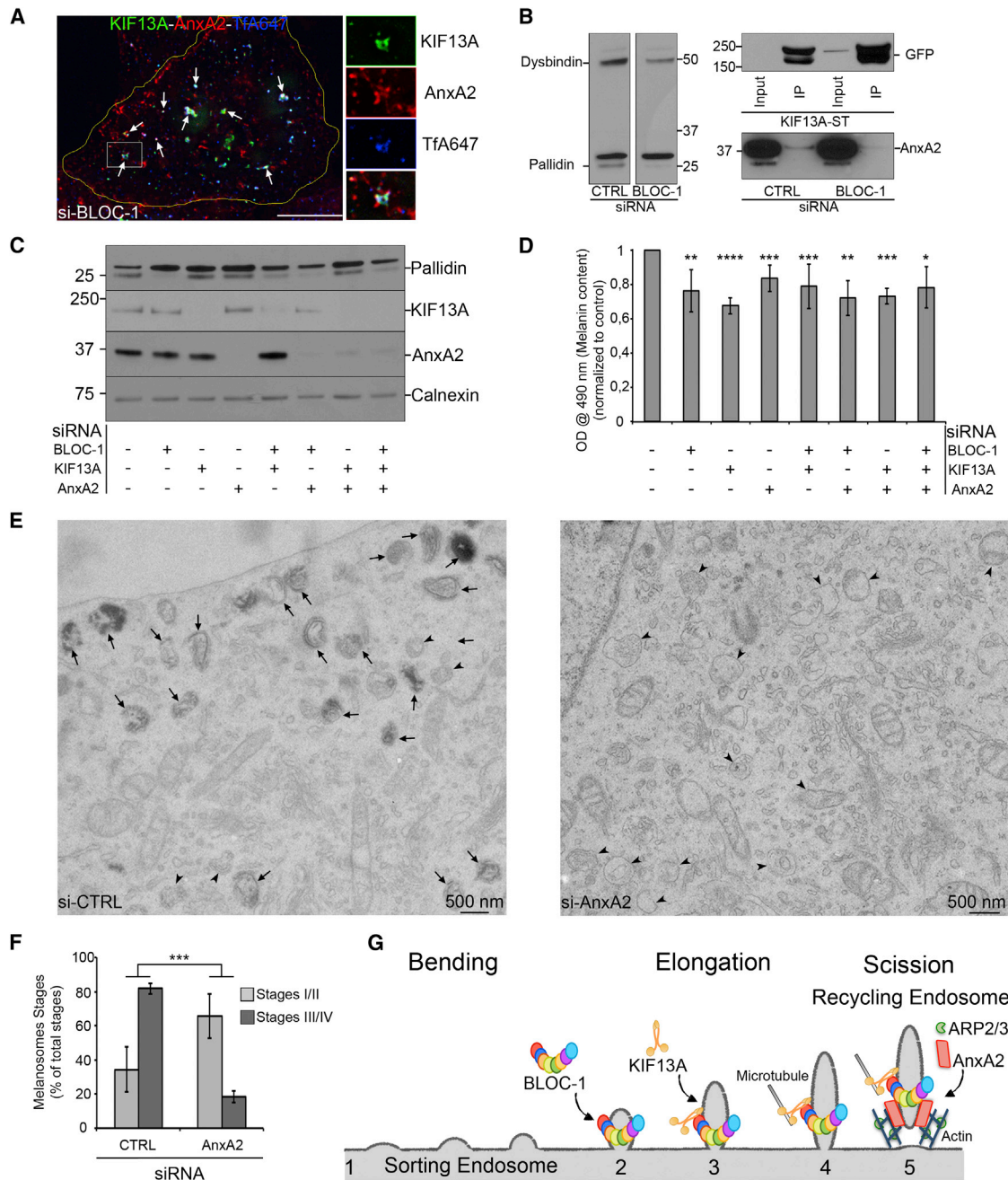
Figure 6. Annexin A2, BLOC-1, and KIF13A Cooperate for Melanosomes Biogenesis

(A) IFM of AnxA2 (red) on KIF13A-expressing (green) siBLOC-1 HeLa cells that internalized TfA647 (blue). Arrows indicate triple KIF13A, AnxA2, and Tf[+] endosomes.

(B) WB representative of three independent IPs of GFP-KIF13A-ST-expressing siCTRL or siBLOC-1 HeLa cells lysates (left) analyzed using GFP (top right) or AnxA2 (bottom right) antibodies. Lower AnxA2 amount is revealed in siBLOC-1 IP while greater KIF13A-ST was immunoprecipitated relative to controls.

(C) WB of siRNA-treated MNT1 lysates using pallidin (top), KIF13A (middle top), AnxA2 (middle bottom), or calnexin (bottom) antibodies.

(D) Intracellular melanin quantification of MNT1 cells as in (C).

(E) Conventional EM analysis of siCTRL or siAnxA2 MNT1 cells. Arrowheads indicate immature melanosome stages I/II; arrows indicate mature pigmented melanosome stages III/IV.

(F) Quantification of melanosome stages in siCTRL or siAnxA2 MNT1 cells.

(G) Model of recycling endosomes shaping by BLOC-1. BLOC-1 binds to highly curved SE membrane deformations (1–2). KIF13A interacts with BLOC-1 at the newly formed tubule (3) and generates the pulling force to elongate the RE tubule from SE (4). AnxA2 binds to SE elongated bud, promotes the ARP2/3-dependent polymerization of branched actin filaments, and participates to the stabilization and/or scission of RE tubules (5).

Data represent the average of at least three independent experiments, normalized to control, and presented as mean ± SD. Scale bars represent 500 nm (EM) and 10 μm (IFM). ****$p < 0.001$; ***$p < 0.01$; **$p < 0.02$; *$p < 0.05$.

(4), whereas AnxA2 and actin polymerization likely participate in the scission of the RE intermediates from SEs in HeLa cells (5) or in RE tubule stabilization in melanocytes where RE intermediates are stably connected to SEs [12, 26]. BLOC-1 bridges the gap between the tubular membrane and microtubules via its interaction with KIF13A and between the two cytoskeletons by stabilizing AnxA2-KIF13A complexes.

Despite the ubiquitous expression of BLOC-1, disruption of BLOC-1 function only manifests with overt phenotypes in a subset of cell types like melanocytes, platelets, and neurons. This reflects the non-redundant function of BLOC-1 in the trafficking of specific cargoes, such as TYRP1, OCA2, and ATP7A in melanocytes [13–15] or dopamine receptor and synaptic vesicle proteins in neurons [48]. Patients or related mouse models of HPS types 7–9 harboring BLOC-1 mutations suffer from albinism and excessive bleeding [11] and are associated with increased risk of schizophrenia [48]. *KIF13A* is a candidate gene for schizophrenia [18], and *Kif13a*$^{-/-}$ mice develop a neurological disorder reflected by elevated anxiety [20]. Our study suggests that the function of the AnxA2-BLOC-1-KIF13A network in shaping RE membrane tubules is a common underlying basis for the pigmentary and neurological defects observed in this disorder.

EXPERIMENTAL PROCEDURES

Statistical Analysis
Unless specified, statistical differences were evaluated between means taken in pairs by Student's t test adapted for small number of samples. A p value < 0.05 was considered as statistically significant.

Correlative Light and Electron Microscopy
HeLa cells cultured 48 hr in CryoCapsules [27] were treated with CTRL-, BLOC1-, or AnxA2-siRNAs (48 hr) and transfected with KIF3A-YFP encoding plasmids (20 hr). TfA546 uptake was performed 1 hr prior to HPF (HPM100, Leica microsystem), and then cells were freeze substituted (12 hr) with 0.05% uranyl acetate, 0.01% gluraltaldehyde and 1% H_2O in dry acetone and embedded in Lowicryl to preserve the fluorescence in bloc. After CryoCapsules removal from the polymerized Lowicryl bloc [49], cells were sectioned with one 250 nm section followed by two or three 70 nm sections. The 250 nm sections were collected on a glass coverslip, mounted with Hoechst-containing mowiol in PBS medium, and imaged (Te2000 epifluorescence microscope). The 70 nm sections were collected on slot grids, floated on Hoechst solution (20 min), rinsed in distilled H_2O, and stored in dark environment. The fluorescent signal on 70 nm sections is comparable to confocal sections due to the physical thickness of the section allowing accurate identification and imaging of cells. The nucleus shape was used to improve cell relocation, and fluorescent image post-processing was performed to increase the signal-to-noise ratio prior to correlative image registration. The 70 nm sections were post-stained with lead citrate (5 min) and imaged (Tecnai Spirit G2; FEI) at increasing magnifications (2,500× to 15,000×).

SUPPLEMENTAL INFORMATION

Supplemental Information includes Supplemental Experimental Procedures, six figures, and six movies and can be found with this article online at http://dx.doi.org/10.1016/j.cub.2015.11.020.

AUTHOR CONTRIBUTIONS

C.D., G.R., E.M., M.S.M., and V.F. conceived the projects and wrote the manuscript. C.D. designed and carried out most of the experiments. X.H., L.R., F.G.-M., M.K.D., R.A.L., L.D., and A.G. performed experiments. All authors edited the manuscript.

REFERENCES

1. Klumperman, J., and Raposo, G. (2014). The complex ultrastructure of the endolysosomal system. Cold Spring Harb. Perspect. Biol. *6*, a016857.

2. Willingham, M.C., Hanover, J.A., Dickson, R.B., and Pastan, I. (1984). Morphologic characterization of the pathway of transferrin endocytosis and recycling in human KB cells. Proc. Natl. Acad. Sci. USA *81*, 175–179.

3. Grant, B.D., and Donaldson, J.G. (2009). Pathways and mechanisms of endocytic recycling. Nat. Rev. Mol. Cell Biol. *10*, 597–608.

4. Marks, M.S., Heijnen, H.F., and Raposo, G. (2013). Lysosome-related organelles: unusual compartments become mainstream. Curr. Opin. Cell Biol. *25*, 495–505.

5. Anitei, M., and Hoflack, B. (2012). Bridging membrane and cytoskeleton dynamics in the secretory and endocytic pathways. Nat. Cell Biol. *14*, 11–19.

6. Derivery, E., Sousa, C., Gautier, J.J., Lombard, B., Loew, D., and Gautreau, A. (2009). The Arp2/3 activator WASH controls the fission of endosomes through a large multiprotein complex. Dev. Cell *17*, 712–723.

7. Morel, E., Parton, R.G., and Gruenberg, J. (2009). Annexin A2-dependent polymerization of actin mediates endosome biogenesis. Dev. Cell *16*, 445–457.

8. Mim, C., and Unger, V.M. (2012). Membrane curvature and its generation by BAR proteins. Trends Biochem. Sci. *37*, 526–533.

9. Granger, E., McNee, G., Allan, V., and Woodman, P. (2014). The role of the cytoskeleton and molecular motors in endosomal dynamics. Semin. Cell Dev. Biol. *31*, 20–29.

10. Raposo, G., and Marks, M.S. (2007). Melanosomes–dark organelles enlighten endosomal membrane transport. Nat. Rev. Mol. Cell Biol. *8*, 786–797.

11. Wei, A.H., and Li, W. (2013). Hermansky-Pudlak syndrome: pigmentary and non-pigmentary defects and their pathogenesis. Pigment Cell Melanoma Res. *26*, 176–192.

12. Delevoye, C., Hurbain, I., Tenza, D., Sibarita, J.B., Uzan-Gafsou, S., Ohno, H., Geerts, W.J., Verkleij, A.J., Salamero, J., Marks, M.S., and Raposo, G. (2009). AP-1 and KIF13A coordinate endosomal sorting and positioning during melanosome biogenesis. J. Cell Biol. *187*, 247–264.

13. Setty, S.R., Tenza, D., Sviderskaya, E.V., Bennett, D.C., Raposo, G., and Marks, M.S. (2008). Cell-specific ATP7A transport sustains copper-dependent tyrosinase activity in melanosomes. Nature *454*, 1142–1146.

14. Setty, S.R., Tenza, D., Truschel, S.T., Chou, E., Sviderskaya, E.V., Theos, A.C., Lamoreux, M.L., Di Pietro, S.M., Starcevic, M., Bennett, D.C., et al. (2007). BLOC-1 is required for cargo-specific sorting from vacuolar early endosomes toward lysosome-related organelles. Mol. Biol. Cell *18*, 768–780.

15. Sitaram, A., Dennis, M.K., Chaudhuri, R., De Jesus-Rojas, W., Tenza, D., Setty, S.R., Wood, C.S., Sviderskaya, E.V., Bennett, D.C., Raposo, G., et al. (2012). Differential recognition of a dileucine-based sorting signal by AP-1 and AP-3 reveals a requirement for both BLOC-1 and AP-3 in delivery of OCA2 to melanosomes. Mol. Biol. Cell *23*, 3178–3192.

16. Di Pietro, S.M., Falcón-Pérez, J.M., Tenza, D., Setty, S.R., Marks, M.S., Raposo, G., and Dell'Angelica, E.C. (2006). BLOC-1 interacts with BLOC-2 and the AP-3 complex to facilitate protein trafficking on endosomes. Mol. Biol. Cell *17*, 4027–4038.

17. Lee, H.H., Nemecek, D., Schindler, C., Smith, W.J., Ghirlando, R., Steven, A.C., Bonifacino, J.S., and Hurley, J.H. (2012). Assembly and architecture of biogenesis of lysosome-related organelles complex-1 (BLOC-1). J. Biol. Chem. *287*, 5882–5890.

18. Jamain, S., Quach, H., Fellous, M., and Bourgeron, T. (2001). Identification of the human KIF13A gene homologous to Drosophila kinesin-73 and candidate for schizophrenia. Genomics *74*, 36–44.

19. Mullin, A.P., Gokhale, A., Larimore, J., and Faundez, V. (2011). Cell biology of the BLOC-1 complex subunit dysbindin, a schizophrenia susceptibility gene. Mol. Neurobiol. *44*, 53–64.

20. Zhou, R., Niwa, S., Guillaud, L., Tong, Y., and Hirokawa, N. (2013). A molecular motor, KIF13A, controls anxiety by transporting the serotonin type 1A receptor. Cell Rep. *3*, 509–519.

21. Falcón-Pérez, J.M., Starcevic, M., Gautam, R., and Dell'Angelica, E.C. (2002). BLOC-1, a novel complex containing the pallidin and muted proteins involved in the biogenesis of melanosomes and platelet-dense granules. J. Biol. Chem. *277*, 28191–28199.

22. Li, W., Zhang, Q., Oiso, N., Novak, E.K., Gautam, R., O'Brien, E.P., Tinsley, C.L., Blake, D.J., Spritz, R.A., Copeland, N.G., et al. (2003). Hermansky-Pudlak syndrome type 7 (HPS-7) results from mutant dysbindin, a member of the biogenesis of lysosome-related organelles complex 1 (BLOC-1). Nat. Genet. *35*, 84–89.

23. Starcevic, M., and Dell'Angelica, E.C. (2004). Identification of snapin and three novel proteins (BLOS1, BLOS2, and BLOS3/reduced pigmentation) as subunits of biogenesis of lysosome-related organelles complex-1 (BLOC-1). J. Biol. Chem. *279*, 28393–28401.

24. Delevoye, C., Miserey-Lenkei, S., Montagnac, G., Gilles-Marsens, F., Paul-Gilloteaux, P., Giordano, F., Waharte, F., Marks, M.S., Goud, B., and Raposo, G. (2014). Recycling endosome tubule morphogenesis from sorting endosomes requires the kinesin motor KIF13A. Cell Rep. *6*, 445–454.

25. Murk, J.L., Posthuma, G., Koster, A.J., Geuze, H.J., Verkleij, A.J., Kleijmeer, M.J., and Humbel, B.M. (2003). Influence of aldehyde fixation on the morphology of endosomes and lysosomes: quantitative analysis and electron tomography. J. Microsc. *212*, 81–90.

26. Dennis, M.K., Mantegazza, A.R., Snir, O.L., Tenza, D., Acosta-Ruiz, A., Delevoye, C., Zorger, R., Sitaram, A., de Jesus-Rojas, W., Ravichandran, K., et al. (2015). BLOC-2 targets recycling endosomal tubules to melanosomes for cargo delivery. J. Cell Biol. *209*, 563–577.

27. Heiligenstein, X., Heiligenstein, J., Delevoye, C., Hurbain, I., Bardin, S., Paul-Gilloteaux, P., Sengmanivong, L., Régnier, G., Salamero, J., Antony, C., and Raposo, G. (2014). The CryoCapsule: simplifying correlative light to electron microscopy. Traffic *15*, 700–716.

28. Cullinane, A.R., Curry, J.A., Carmona-Rivera, C., Summers, C.G., Ciccone, C., Cardillo, N.D., Dorward, H., Hess, R.A., White, J.G., Adams, D., et al. (2011). A BLOC-1 mutation screen reveals that PLDN is mutated in Hermansky-Pudlak Syndrome type 9. Am. J. Hum. Genet. *88*, 778–787.

29. Prekeris, R., Klumperman, J., Chen, Y.A., and Scheller, R.H. (1998). Syntaxin 13 mediates cycling of plasma membrane proteins via tubulovesicular recycling endosomes. J. Cell Biol. *143*, 957–971.

30. Harbour, M.E., Breusegem, S.Y., and Seaman, M.N. (2012). Recruitment of the endosomal WASH complex is mediated by the extended 'tail' of Fam21 binding to the retromer protein Vps35. Biochem. J. *442*, 209–220.

31. Gerke, V., Creutz, C.E., and Moss, S.E. (2005). Annexins: linking Ca2+ signalling to membrane dynamics. Nat. Rev. Mol. Cell Biol. *6*, 449–461.

32. Emans, N., Gorvel, J.P., Walter, C., Gerke, V., Kellner, R., Griffiths, G., and Gruenberg, J. (1993). Annexin II is a major component of fusogenic endosomal vesicles. J. Cell Biol. *120*, 1357–1369.

33. Zeuschner, D., Stoorvogel, W., and Gerke, V. (2001). Association of annexin 2 with recycling endosomes requires either calcium- or cholesterol-stabilized membrane domains. Eur. J. Cell Biol. *80*, 499–507.

34. Loubéry, S., Delevoye, C., Louvard, D., Raposo, G., and Coudrier, E. (2012). Myosin VI regulates actin dynamics and melanosome biogenesis. Traffic *13*, 665–680.

35. Moreau, K., Ghislat, G., Hochfeld, W., Renna, M., Zavodszky, E., Runwal, G., Puri, C., Lee, S., Siddiqi, F., Menzies, F.M., et al. (2015). Transcriptional regulation of Annexin A2 promotes starvation-induced autophagy. Nat. Commun. *6*, 8045.

36. Zobiack, N., Rescher, U., Ludwig, C., Zeuschner, D., and Gerke, V. (2003). The annexin 2/S100A10 complex controls the distribution of transferrin receptor-containing recycling endosomes. Mol. Biol. Cell *14*, 4896–4908.

37. Ryder, P.V., Vistein, R., Gokhale, A., Seaman, M.N., Puthenveedu, M.A., and Faundez, V. (2013). The WASH complex, an endosomal Arp2/3 activator, interacts with the Hermansky-Pudlak syndrome complex BLOC-1 and its cargo phosphatidylinositol-4-kinase type IIα. Mol. Biol. Cell *24*, 2269–2284.

38. Maxfield, F.R., and McGraw, T.E. (2004). Endocytic recycling. Nat. Rev. Mol. Cell Biol. *5*, 121–132.

39. Pu, J., Schindler, C., Jia, R., Jarnik, M., Backlund, P., and Bonifacino, J.S. (2015). BORC, a multisubunit complex that regulates lysosome positioning. Dev. Cell *33*, 176–188.

40. Setou, M., Nakagawa, T., Seog, D.H., and Hirokawa, N. (2000). Kinesin superfamily motor protein KIF17 and mLin-10 in NMDA receptor-containing vesicle transport. Science *288*, 1796–1802.

41. Matus, A. (2000). Actin-based plasticity in dendritic spines. Science *290*, 754–758.

42. Idrissi, F.Z., Blasco, A., Espinal, A., and Geli, M.I. (2012). Ultrastructural dynamics of proteins involved in endocytic budding. Proc. Natl. Acad. Sci. USA *109*, E2587–E2594.

43. Kukulski, W., Schorb, M., Kaksonen, M., and Briggs, J.A. (2012). Plasma membrane reshaping during endocytosis is revealed by time-resolved electron tomography. Cell *150*, 508–520.

44. Monfregola, J., Napolitano, G., D'Urso, M., Lappalainen, P., and Ursini, M.V. (2010). Functional characterization of Wiskott-Aldrich syndrome protein and scar homolog (WASH), a bi-modular nucleation-promoting factor able to interact with biogenesis of lysosome-related organelle subunit 2 (BLOS2) and gamma-tubulin. J. Biol. Chem. *285*, 16951–16957.

45. Mayran, N., Parton, R.G., and Gruenberg, J. (2003). Annexin II regulates multivesicular endosome biogenesis in the degradation pathway of animal cells. EMBO J. *22*, 3242–3253.

46. Morel, E., and Gruenberg, J. (2007). The p11/S100A10 light chain of annexin A2 is dispensable for annexin A2 association to endosomes and functions in endosomal transport. PLoS ONE *2*, e1118.

47. John Peter, A.T., Lachmann, J., Rana, M., Bunge, M., Cabrera, M., and Ungermann, C. (2013). The BLOC-1 complex promotes endosomal maturation by recruiting the Rab5 GTPase-activating protein Msb3. J. Cell Biol. *201*, 97–111.

48. Ryder, P.V., and Faundez, V. (2009). Schizophrenia: the "BLOC" may be in the endosomes. Sci. Signal. *2*, pe66.

49. Heiligenstein, X., Hurbain, I., Delevoye, C., Salamero, J., Antony, C., and Raposo, G. (2014). Step by step manipulation of the CryoCapsule with HPM high pressure freezers. Methods Cell Biol. *124*, 259–274.